Communication

Effect of Interfacial Mn Partitioning on Carbon Partitioning and Interface Migration During the Quenching and Partitioning Process

ZONGBIAO DAI, XU WANG, JIANGUO HE, ZHIGANG YANG, CHI ZHANG , and HAO CHEN

A so-called QP-LE model, in which interface condition is assumed to be Local Equilibrium (LE), has been proposed to evaluate the effect of interfacial Mn partitioning on interface migration and carbon partitioning during the Quenching and partitioning process (Q&P) of an Fe-0.3C-3.0Mn-1.5Si (wt pct) alloy. The predictions by the QP-LE model are compared with those by the conventional QP-PE model in which interface condition is assumed to be Paraequilibrium (PE). It is found that interfacial partitioning of Mn plays a significant role in carbon partitioning and the martensite/austenite interface migration during the Q&P process.

DOI: 10.1007/s11661-017-4121-y

Quenching and Partitioning (Q&P) has been proven to be an effective approach to increase the fraction of retained austenite in the advanced high strength steels, and it has received extensive attention from physical metallurgists.[1–3] Despite its great practical importance, the underlying physics of substitutional alloying element effects on the martensite/austenite (α'/γ) interface migration and carbon partitioning during the Q&P process is still not well understood. The partitioning process was initially assumed to proceed in the Constrained Carbon Equilibrium (CCE), in which the α'/γ interface was considered to be immobile while carbon has equal chemical potential in martensite and austenite.[1,2] The α'/γ interface has been experimentally found to be immobile during the Q&P process.[4–6] However, some recent studies directly or indirectly indicated that the α'/γ interface could be mobile during the Q&P process, while the direction of interface migration was found to vary in different experiments.[7–11]

A sophisticated model was proposed to simulate carbon partitioning and interface migration during the partitioning process in the binary Fe-C system, and it predicted that the α'/γ interface could migrate in either direction.[12,13] This model was further applied to multi-component alloys assuming Paraequilibrium (PE) at the interface, *e.g.*, substitutional alloying elements (X) do not partition at the interface,[10,14] and it could well describe the kinetics of the α'/γ interface migration by assuming a much lower interface mobility than that for the austenite to ferrite transformation. This interface mobility can be considered as an effective interface mobility.[10,15] With the rapid development of three-dimensional atom probe tomography (3D-APT), nanoscale partitioning of X was recently detected at the α'/γ interface after the Q&P process by several research groups.[4–6,16,17] It has been experimentally and theoretically proven that interfacial partitioning of X could play a significant role in the kinetics of interface migration and carbon partitioning during the austenite to ferrite transformation and bainitic transformation.[18–23] It is speculated that the interfacial partitioning of X could also affect the kinetics of interface migration and carbon partitioning during the Q&P process.

In the current study, a so-called QP-LE model, in which interface condition is assumed to be Local Equilibrium (LE), has been proposed to investigate the effects of interfacial Mn partitioning on the α'/γ interface migration and carbon partitioning during the Q&P process in the Fe-0.3C-3.0Mn-1.5Si (wt pct) alloy. The values of the intrinsic interface mobility in both LE and PE models are assumed to be infinite, and a comparison between them is made.

In the PE model,[24,25] it is assumed that during phase transformations the interface migrates without any redistribution of substitutional alloying elements (X) between ferrite (α) and austenite (γ) phases, whereas carbon has equal chemical potential across the interface. Hence, the kinetics of interface migration is controlled by carbon diffusion. The constraint equilibrium can be expressed as:

$$\mu_C^{\gamma} = \mu_C^{\alpha}, \qquad [1]$$

$$\mu_X^{\gamma} - \mu_X^{\alpha} = -\frac{x_{Fe}}{x_X}(\mu_{Fe}^{\gamma} - \mu_{Fe}^{\alpha}), \qquad [2]$$

where μ_i^{α} and μ_i^{γ} are chemical potential of element i (i = Fe, C, or X) at the interface in α and γ phase, respectively, and $\frac{x_{Fe}}{x_X}$ is the constant ratio of the Fe to X concentration across the interface.

ZONGBIAO DAI, JIANGUO HE, ZHIGANG YANG, CHI ZHANG, and HAO CHEN are with the Key Laboratory for Advanced Materials, Ministry of Education, School of Materials Science and Engineering, Tsinghua University, Beijing 100084, China. Contact e-mail: hao.chen@mail.tsinghua.edu.cn XU WANG is with the Technology Center of Ansteel Corporation, Wuyi Road 63, Anshan 114009, China.

Manuscript submitted October 26, 2016.
Article published online May 8, 2017

In the LE model,[26–28] both C and X are assumed to redistribute at the interface according to the LE condition, *e.g.*, the chemical potentials of C and X should be constant across the interface:

$$\mu_i^{\gamma} = \mu_i^{\alpha} \qquad (i = Fe, C, X) \qquad [3]$$

Due to the large difference between diffusion coefficients of C and X, two modes of interface migration are expected to occur under the LE condition: Negligible Partitioning-Local Equilibrium (NPLE) and Partitioning-Local Equilibrium (PLE). In Figure 1(a) and (b), the isothermal sections of the ternary Fe-C-X phase diagram are shown to illustrate the NPLE/PLE boundary AB for the austenite (γ) to ferrite (α) transformation. When alloy composition (point O) lies below line AB, interface migration mode is NPLE and it is controlled by C diffusion. As shown in Figure 1(a), there is no redistribution of X while a spike of X will appear ahead of the migrating interface, and X content in α is identical to bulk composition. With the formation of α and C enrichment in γ, C content in γ will change gradually from point O to R. As shown in Figure 1(b), when the carbon content in γ reaches the value that was determined by point R, interface migration changes into the PLE mode and it is controlled by X diffusion.[29] In the PLE mode, C content gradient in both α and γ is negligible while X content gradient in γ is still greater. In Figure 1(c) and (d), the isothermal sections of the ternary Fe-C-X phase diagram are shown to illustrate the NPLE/PLE boundary for the ferrite (α) to austenite (γ) transformation. It should be emphasized that the NPLE/PLE boundary AB for the $\alpha \rightarrow \gamma$ transformation is different from that for the $\gamma \rightarrow \alpha$ transformation. Compared with the $\gamma \rightarrow \alpha$ transformation, kinetic transition between NPLE and PLE during the $\alpha \rightarrow \gamma$ transformation was relatively less investigated.[30–33]

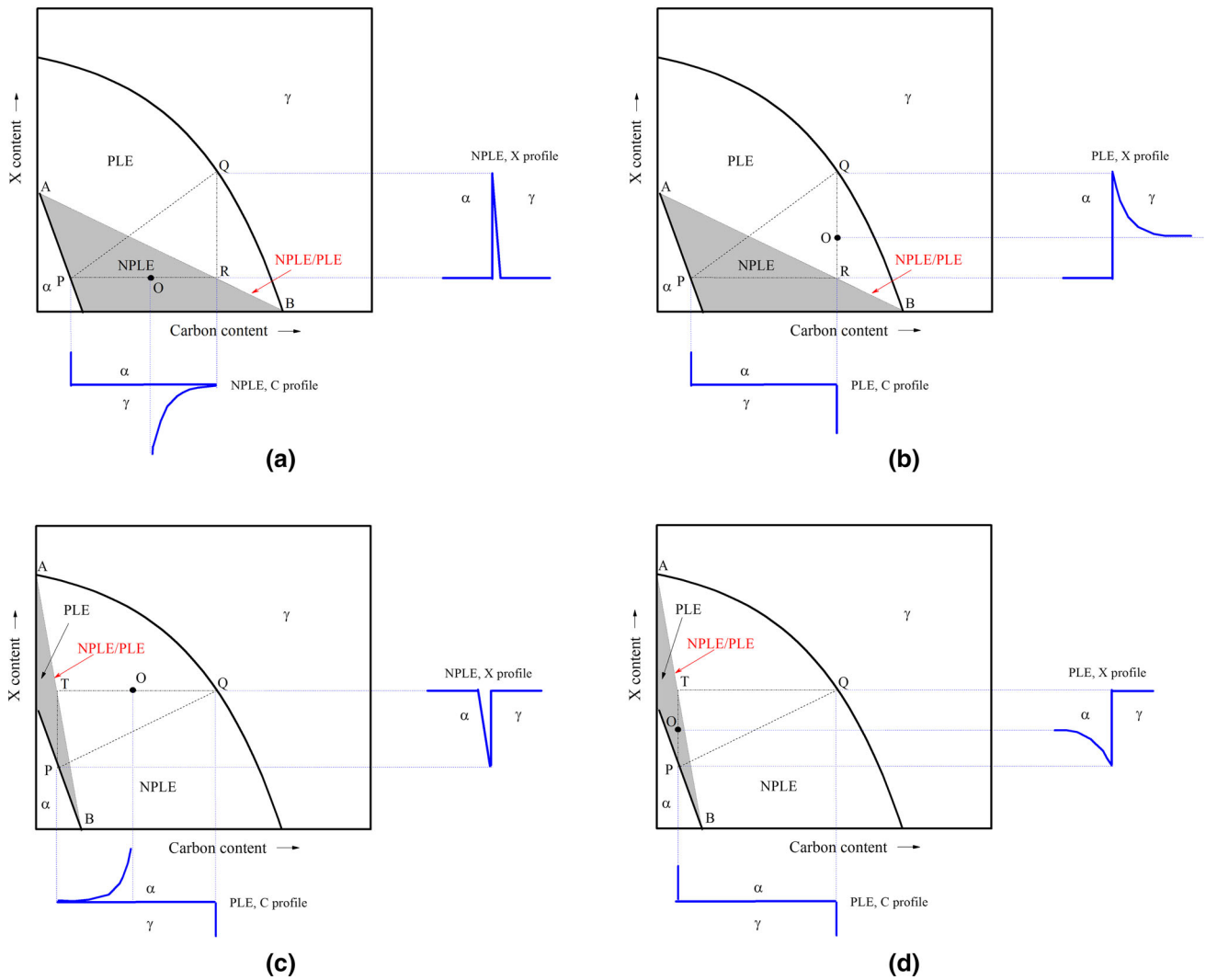

Fig. 1—Isothermal sections of ternary Fe-C-X phase diagram (X is substitutional alloying element). (*a*) NPLE mode for the $\gamma \rightarrow \alpha$ transformation when O is below AB; (*b*) PLE mode for the $\gamma \rightarrow \alpha$ transformation when O is above AB; (*c*) NPLE mode for the $\alpha \rightarrow \gamma$ transformation when O is on the right of AB; (*d*) PLE mode for the $\alpha \rightarrow \gamma$ transformation when O is on the left of AB.

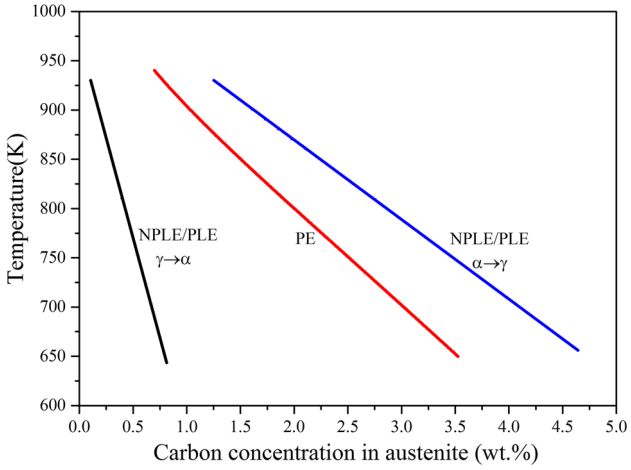

Fig. 2— $\gamma/(\alpha+\gamma)$ phase boundaries under the PE and LE condition for Fe-0.3C-3.0Mn-1.5Si (wt pct).

In this study, in order to investigate the influence of quenching temperature (QT) on interface migration and carbon partitioning during the Q&P process, partitioning temperature (PT) is fixed at 673 K (400 °C), while QT varies from 371 K to 540 K (98 °C to 267 °C). Fraction of austenite prior to the partitioning process is determined by QT, and it can be estimated using the Koistinen–Marburger (K-M) equation.[34,35] The simulated object is austenite–martensite grain assemblies with a film morphology, and the total thickness of them is assumed to be 300nm. The QP-PE and QP-LE models are both applied to investigate carbon partitioning and interface migration during the Q&P process, and a comparison between them is made. Figure 2 shows $\gamma/(\alpha+\gamma)$ phase boundaries, which refer to the peak C content in the austenite at the α/γ interface, under the PE and LE condition for Fe-0.3C-3.0Mn-1.5Si(wt pct). The NPLE/PLE and PE $\gamma/(\alpha+\gamma)$ boundaries below 773 K (500 °C) are linearly extrapolated from those at

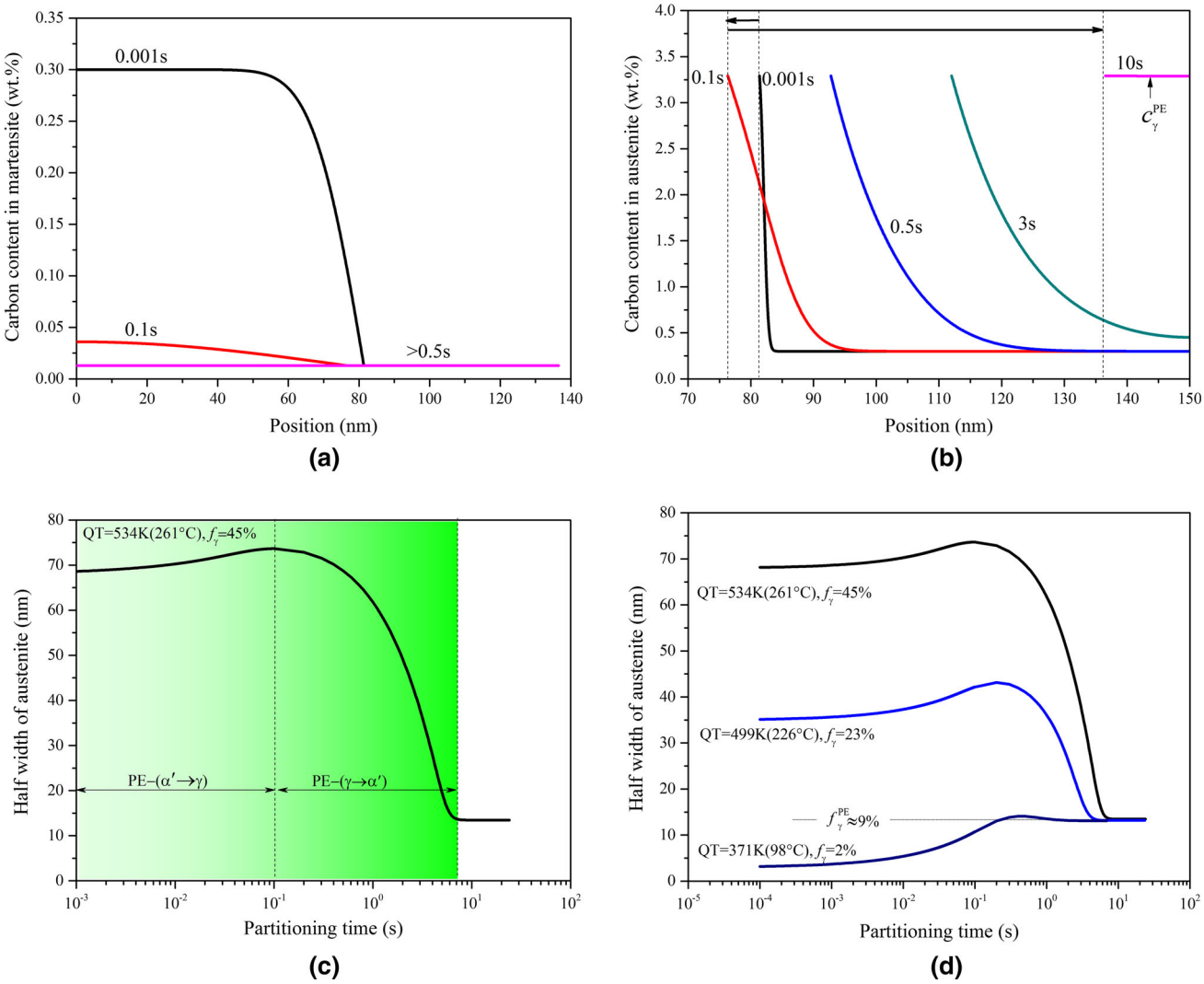

Fig. 3—The evolution of carbon profiles in (*a*) martensite and (*b*) austenite; the half width of austenite as a function of time during partitioning at 673 K (400 °C) and (*c*) quenched to 534 K (261 °C) and (*d*) quenched to various temperatures. Arrows in (b) indicate the direction of interface migration. Interface condition is assumed to be Paraequilibrium.

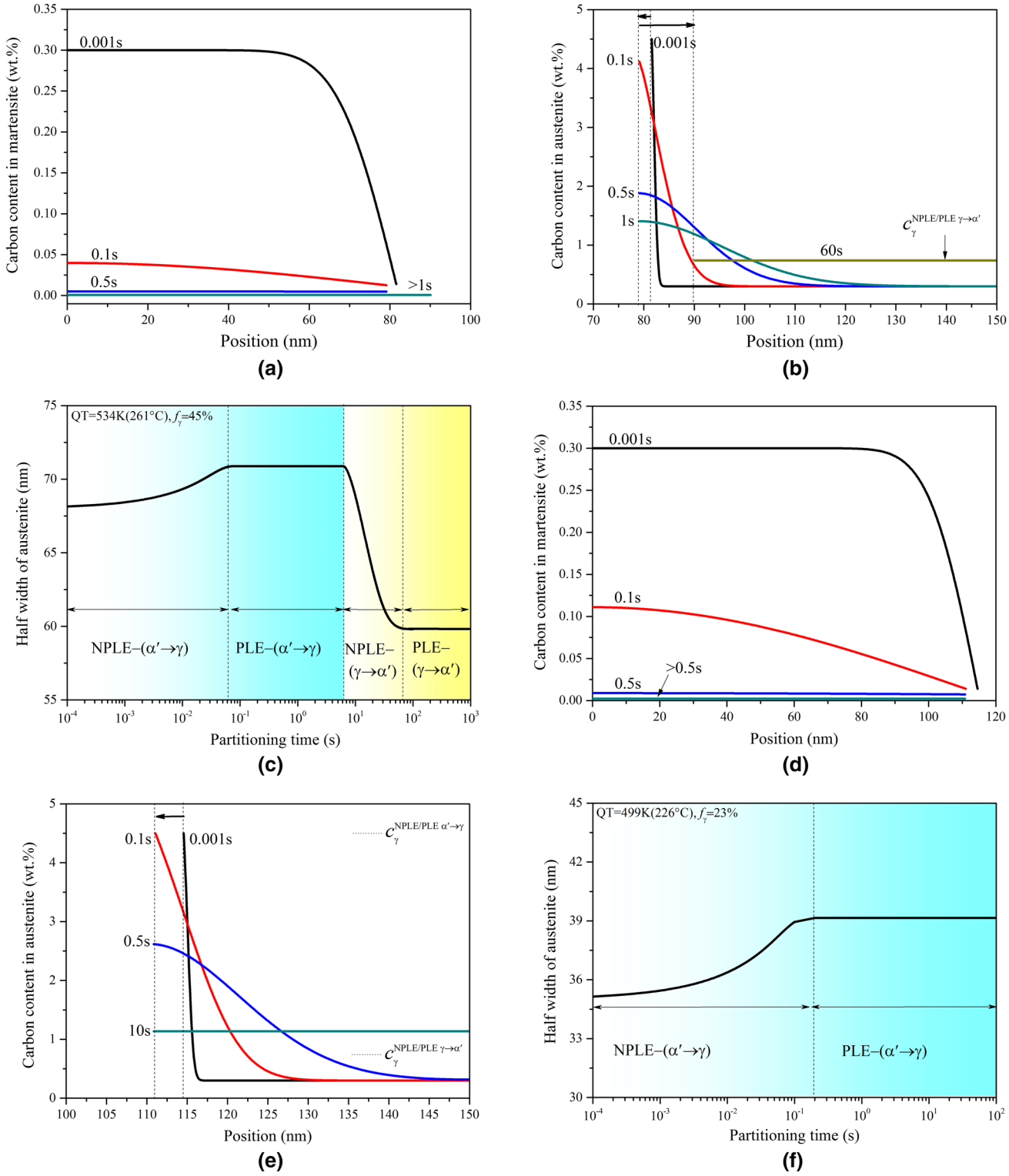

Fig. 4—The carbon profiles in martensite (*a*, *d*) and austenite (*b*, *e*) together with the corresponding half width of austenite (*c*, *f*) as a function of time during partitioning at 673 K (400 °C) for this alloy quenched to 534 K and 499 K (261 °C and 226 °C); (*g*) the half width of austenite as a function of partitioning time for this alloy quenched to various temperatures and followed by partitioning at 673 K (400 °C); (*h*) Carbon concentration in austenite at the stasis state as a function of QT. Arrows in (b) and (e) indicate the direction of interface migration. Interface condition is assumed to be Local Equilibrium.

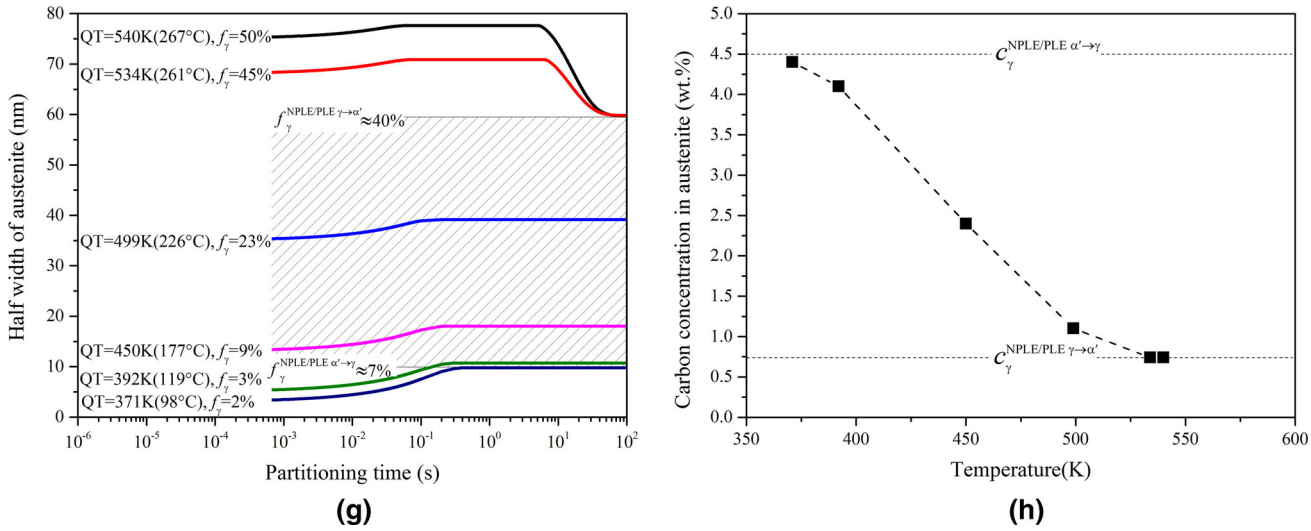

Fig. 4—continued.

elevated temperatures [above 773 K (500 °C)] due to the absence of appropriate thermodynamic data at low temperatures in Thermo-Calc.[36]

Figure 3(a) and (b) show the evolution of carbon profiles in martensite and austenite during partitioning at 673 K (400 °C) after quenching to 534 K (261 °C), and the corresponding half width of austenite as a function of time is shown in Figure 3(c). The calculations are made by the QP-PE model. The partitioning process can be divided into two stages: (i) the PE- ($\alpha' \rightarrow \gamma$) transformation stage (~0.1 seconds), in which carbon in martensite escapes very quickly into austenite, and is then enriched at the interface on the austenite side since the diffusivity of carbon in martensite is much higher than that in austenite. As shown in Figure 3(c), in this stage the interface is predicted to migrate toward martensite, and interface migration is controlled by carbon diffusion in martensite; (ii) the PE- ($\gamma \rightarrow \alpha'$) transformation stage (0.1~7 seconds). In this stage, carbon profiles in martensite almost do not change while those in austenite are gradually approaching homogenization and finally reach the PE state. In this stage, the interface migrates backward into austenite.

In order to analyze the effect of QT on interface migration during the partitioning process, three simulations have been made by the QP-PE model: PT is fixed at 673 K (400 °C), while QTs are 534 K, 499 K, and 371 K (261 °C, 226 °C, and 98 °C). In Figure 3(d), the calculated half width of austenite as a function of time during partitioning at 673 K (400 °C) is shown. The initial PE- ($\alpha' \rightarrow \gamma$) transformation stage has been predicted to occur in all cases, while the presence of the PE- ($\gamma \rightarrow \alpha'$) transformation stage or not is QT dependent, *e.g.*, the PE- ($\gamma \rightarrow \alpha'$) transformation is almost absent when the QT is 371 K (98 °C). However, it has to be emphasized that the final austenite fraction and carbon concentration in austenite are not influenced by QT according to the QP-PE model, which contradicts the previous experimental results.[1,6]

Figure 4(a) and (b) show the evolution of carbon profiles in martensite and austenite during partitioning at 673 K (400 °C) after quenching to 534 K (261 °C), and the corresponding half width of austenite as a function of time is shown in Figure 4(c). The partitioning process predicted by the QP-LE model can be divided into four stages: (i) The NPLE- ($\alpha' \rightarrow \gamma$) transformation stage (~0.06 seconds). In this stage, the interface migrates into martensite at a very high rate, and carbon escapes quickly from martensite into austenite. The interface migration is controlled by carbon diffusion in martensite; (ii) The PLE- ($\alpha' \rightarrow \gamma$) transformation stage (0.06~6 seconds). According to mass balance at the interface, the interface velocity in this stage is determined by Mn and Si diffusion. Due to the diffusion coefficients of Mn and Si being very small, the interface velocity in this stage is extremely slow. The sharp carbon profile in austenite developed during the NPLE- ($\alpha' \rightarrow \gamma$) stage is diffusing out, and carbon concentration at the interface on the austenite side gradually approaches the NPLE/PLE boundary for the $\gamma \rightarrow \alpha'$ transformation; (iii) The NPLE- ($\gamma \rightarrow \alpha'$) transformation stage (6~60 seconds). In this stage, the interface migrates into austenite substantially, and its kinetics is controlled by carbon diffusion in austenite. Carbon profiles in martensite almost do not change while carbon concentration in austenite is homogenizing and gradually reaches the NPLE/PLE boundary for the $\gamma \rightarrow \alpha'$ transformation; (iv) The PLE- ($\gamma \rightarrow \alpha'$) transformation stage (60 seconds ~), in which interface migration is Mn and Si diffusion controlled and carbon concentration in austenite is homogeneous. In this stage, interface migration has reached a stasis state, which means the interface is continuing to move at an extremely slow rate. Carbon concentration in austenite at the stasis is $c_\gamma^{NPLE/PLE\gamma\rightarrow\alpha'}$, which is determined by the NPLE/PLE boundary for the $\gamma \rightarrow \alpha'$ transformation. Figure 4(d) and (e) show the evolution of carbon profiles

in martensite and austenite during partitioning at 673 K (400 °C) after quenching to 499 K (226 °C), and the corresponding half width of austenite as a function of time is shown in Figure 4(f). In this situation, only two stages are predicted to occur during the partitioning process: (i) The NPLE- ($\alpha' \rightarrow \gamma$) transformation stage (~0.2 seconds), during which carbon diffuses from martensite into austenite, and the interface moves into martensite; (ii) The PLE- ($\alpha' \rightarrow \gamma$) transformation stage (0.2 seconds ~), in which carbon concentration in austenite reaches homogenization quickly as the initial fraction of austenite is small, and interface migration has reached a stasis state. Carbon concentration in austenite at the stasis for this case is located between $c_{\gamma}^{NPLE/PLE\gamma\rightarrow\alpha'}$ and $c_{\gamma}^{NPLE/PLE\alpha'\rightarrow\gamma}$. It is worth noting that although interface migration in the PE and NPLE mode are both controlled by carbon diffusion, interface contact conditions of them are different, which leads to different kinetics of interface migration and carbon concentration in austenite.

Figure 4(g) shows the half width of austenite as a function of time during partitioning at 673 K (400 °C) after quenching to various temperatures. Similar to the predictions by the QP-PE model, the initial $\alpha' \rightarrow \gamma$ stage is predicted to occur for all cases, and the presence of the $\gamma \rightarrow \alpha'$ stage or not is QT dependent. Different from the QP-PE predictions, the final width of austenite and carbon concentration in austenite at the stasis depends strongly on QT according to the QP-LE model. As shown in Figure 4(h), the lower and upper limits of carbon concentration in austenite at the stasis predicted by the QP-LE model are $c_{\gamma}^{NPLE/PLE\gamma\rightarrow\alpha'}$ and $c_{\gamma}^{NPLE/PLE\alpha'\rightarrow\gamma}$. It is worth noting that carbon concentration in austenite can hardly reach the upper limit in reality as carbide is expected to form if carbon concentration is very high. Carbide precipitation can consume significant amounts of carbon and then reduce the austenite fraction at the stasis state based on the level rule.[37–40] The influence of carbide precipitation on interface migration and carbon partitioning needs to be further investigated in a 2D or 3D model. This study is focused on the effect of Mn partitioning. Solute drag effects caused by Mn is not considered in the current model. However, it has been indicated that the LE model's predictions for the Fe-C-Mn alloys are almost the same as those by the so-called GEB model considering solute drag effects.[41]

In summary, kinetics of interface migration and alloying element partitioning during the partitioning process are strongly dependent on the assumed interface condition, and the key differences between the QP-PE and QP-LE models are summarized as following:

(i) Kinetics of interface migration. Based on the QP-LE model, the kinetics of interface migration during the partitioning process can be generally divided into four stages: NPLE- ($\alpha' \rightarrow \gamma$) → PLE- ($\alpha' \rightarrow \gamma$) → NPLE- ($\gamma \rightarrow \alpha'$) → PLE- ($\gamma \rightarrow \alpha'$). Presence of the NPLE- ($\gamma \rightarrow \alpha'$) and PLE- ($\gamma \rightarrow \alpha'$) stages or not depends on QT. However, the interface is expected to migrate firstly in the PE- ($\alpha' \rightarrow \gamma$) mode and then the PE- ($\gamma \rightarrow \alpha'$) mode according to the QP-PE model.

(ii) Alloying element partitioning. After the partitioning process (*e.g.*, the interface migration has reached the stasis state), carbon concentration in austenite should reach the PE boundary according to the QP-PE model, while it could be located between the NPLE/PLE boundaries for the $\gamma \rightarrow \alpha'$ transformation and the $\alpha' \rightarrow \gamma$ transformation based on the QP-LE model. Substitutional alloying element partitioning across the interface is predicted to occur by the QP-LE model but not by the QP-PE model.It is should be emphasized that the QP-LE model needs to be further benchmarked in the future, although interfacial partitioning of substitutional alloying elements has been detected by several research groups.[4–6,16,17]

H. Chen acknowledges financial support from National Natural Science Foundation of China (51501099) and National Young 1000-Talents Program (D1101073), and ZG Yang acknowledges the support from the National Natural Science Foundation of China (Grant 51471094).

REFERENCES

1. J.G. Speer, D.K. Matlock, B.C. De Cooman, and J.G. Schroth: *Acta Mater.*, 2003, vol. 51, pp. 2611–22.
2. J.G. Speer, D.V. Edmonds, F.C. Rizzo, and D.K. Matlock: *Curr. Opin. Solid State Mater. Sci.*, 2004, vol. 8, pp. 219–37.
3. J.G. Speer, E. De Moor, and A.J. Clark: *Mater. Sci. Technol.*, 2015, vol. 31, pp. 3–9.
4. Y. Toji, H. Matsuda, M. Herbig, P.-P. Choi, and D. Raabe: *Acta Mater.*, 2014, vol. 65, pp. 215–28.
5. E.J. Seo, L. Cho, and B.C. De Cooman: *Acta Mater.*, 2016, vol. 107, pp. 354–65.
6. E.J. Seo, L. Cho, Y. Estrin, and B.C. De Cooman: *Acta Mater.*, 2016, vol. 113, pp. 124–39.
7. N. Zhong, X.D. Wang, Y.H. Rong, and L. Wang: *J. Mater. Sci. Technol.*, 2006, vol. 22, pp. 751–54.
8. M.J. Santofimia, L. Zhao, and J. Sietsma: *Metall. Mater. Trans. A*, 2011, vol. 42A, pp. 3620–26.
9. M.J. Santofimia, L. Zhao, R. Petrov, C. Kwakernaak, W.G. Sloof, and J. Sietsma: *Acta Mater.*, 2011, vol. 59, pp. 6059–68.
10. D. De Knijf, M.J. Santofimia, H. Shi, V. Bliznuk, C. Föjer, R. Petrov, and W. Xu: *Acta Mater.*, 2015, vol. 90, pp. 161–68.
11. G.A. Thomas and J.G. Speer: *Mater. Sci. Technol.*, 2014, vol. 30, pp. 998–1007.
12. M.J. Santofimia, L. Zhao, and J. Sietsma: *Scr. Mater.*, 2008, vol. 59, pp. 159–62.
13. M.J. Santofimia, J.G. Speer, A.J. Clarke, L. Zhao, and J. Sietsma: *Acta Mater.*, 2009, vol. 57, pp. 4548–57.
14. Y. Takahama, M.J. Santofimia, M.G. Mecozzi, L. Zhao, and J. Sietsma: *Acta Mater.*, 2012, vol. 60, pp. 2916–26.
15. E. Gamsjäger, H. Chen, and S. van der Zwaag: *Comput. Mater. Sci.*, 2014, vol. 83, pp. 92–100.
16. M.J. Santofimia, L. Zhao L, I. Povstugar, P.-P. Choi, D. Raabe, and J. Sietsma: 3rd International Symposium Steel Science, The Iron and Steel Institute of Japan, Kyoto, 2012, pp. 155–58.
17. X. Zhu, W. Li, H.S. Zhao, L. Wang, and X.J. Jin: *Int. J. Hydrog. Energy*, 2014, vol. 39, pp. 13031–40.
18. M. Enomoto: *Acta Mater.*, 1999, vol. 47, pp. 3533–40.

19. H.S. Zurob, C.R. Hutchinson, A. Béché, G.R. Purdy, and Y.J.M. Bréchet: *Acta Mater.*, 2008, vol. 56, pp. 2203–11.
20. C. Qiu, H.S. Zurob, and C.R. Hutchinson: *Acta Mater.*, 2015, vol. 100, pp. 333–43.
21. H. Chen, A. Borgenstam, J. Odqvist, I. Zuazo, M. Goune, J. Ågren, and S. van der Zwaag: *Acta Mater.*, 2013, vol. 61, pp. 4512–23.
22. K.Y. Zhu, H. Chen, J.-P. Masse, O. Bouaziz, and G. Gachet: *Acta Mater.*, 2013, vol. 61, pp. 6025–36.
23. H. Chen and S. van der Zwaag: *JOM*, 2016, vol. 68, pp. 1320–28.
24. A. Hultgren: *Trans. ASM*, 1947, vol. 39, pp. 915–22.
25. M. Hillert: Introduction to Paraequilibrium, Internal Report, Swedish Institute of Metals Research, Stockholm, 1953.
26. C. Zener: *J. Appl. Phys.*, 1949, vol. 20, pp. 950–53.
27. J.S. Kirkaldy: *Can. J. Phys.*, 1958, vol. 36, pp. 907–16.
28. D.E. Coates: *Metall. Trans.*, 1972, vol. 3, pp. 1203–12.
29. A. Van der Ven and L. Delaey: *Prog. Mater. Sci.*, 1996, vol. 40, pp. 181–264.
30. H.W. Luo, J. Shi, C. Wang, W.Q. Cao, X.J. Sun, and H. Dong: *Acta Mater.*, 2011, vol. 59, pp. 4002–14.
31. H. Chen, W. Xu, M. Gouné, and S. van der Zwaag: *Philos. Mag. Lett.*, 2012, vol. 92, pp. 547–55.
32. R. Wei, M. Enomoto, R. Hadian, H.S. Zurob, and G.R. Purdy: *Acta Mater.*, 2013, vol. 61, pp. 697–707.
33. N. Nakada, K. Mizutani, T. Tsuchiyama, and S. Takaki: *Acta Mater.*, 2014, vol. 65, pp. 251–58.
34. D.P. Koistinen and R.E. Marburger: *Acta Metall.*, 1959, vol. 7, pp. 59–60.
35. S.M.C. Van Bohemen: *Mater. Sci. Technol.*, 2012, vol. 28, pp. 487–95.
36. Thermo-Calc is trademark of Thermo-Calc software. http://www.thermocalc.com/.
37. Y. Toji, G. Miyamoto, and D. Rabbe: *Acta Mater.*, 2015, vol. 86, pp. 137–47.
38. D.T. Pierce, D.R. Coughlin, D.L. Williamson, K.D. Clarke, A.J. Clarke, J.G. Speer, and E. De Moor: *Acta Mater.*, 2015, vol. 90, pp. 417–30.
39. D.T. Pierce, D.R. Coughlin, D.L. Williamson, J. Kähkönen, A.J. Clarke, K.D. Clarke, J.G. Speer, and E. De Moor: *Scr. Mater.*, 2016, vol. 121, pp. 5–9.
40. D.V. Edmonds, K. He, F.C. Rizzo, B.C. De Cooman, D.K. Matlock, and J.G. Speer: *Mater. Sci. Eng. A*, 2006, vols. 438–440, pp. 25–34.
41. H. Chen and S. van der Zwaag: *Acta Mater.*, 2014, vol. 72, pp. 1–12.